JOURNAL OF SPACECRAFT AND ROCKETS
Vol. 38, No. 2, March–April 2001

Design of Space Launch Vehicle Using Numerical Optimization and Inverse Method

Jae-Woo Lee,* Young-Ki Lee,† and Yung-Hwan Byun‡
Konkuk University, Seoul 143-701, Republic of Korea
and
Ho-Yon Hwang§
Sejong University, Seoul 143-747, Republic of Korea

The inverse method and the numerical optimization technique are developed and implemented for the design of space launch vehicles, which satisfy given heat transfer rate, fineness ratio and internal volume constraints, and show minimum drag characteristics. With the proper specification of the target pressure distribution, the inverse method is successfully applied to the design of a body with 21% less drag than the initial shape. Several gradient approximations, shape functions, and approximate analysis methods are utilized for the design of optimum nose fairing shapes with heat flux and volume constraints. Several strategies are implemented to the design examples in hypersonic speeds, including a Korean three-stage sounding rocket. The designed bodies have less drag than the initial bodies while maintaining the surface heat transfer rate at the nose. These methods are demonstrated to be efficient design tools for the high-speed vehicle design.

Nomenclature

C_D	=	drag coefficient
C_h	=	Stanton number
C_p	=	pressure coefficient
d	=	base diameter of the body, m
H_{aw}	=	total enthalpy at adiabatic wall temperature
H_w	=	total enthalpy at wall
l	=	body length, m
M_∞	=	freestream Mach number
n	=	exponent of the power law body
Pr	=	Prandtl number
p_∞	=	freestream static pressure, N/m^2
q	=	heat flux, W/m^2
q_w	=	heat flux at the wall
R	=	body radius, normalized by body length
R_n	=	nose radius of curvature
R_θ	=	momentum thickness Reynolds number
T_∞	=	freestream temperature, K
u	=	velocity component in x direction, m/s
x	=	longitudinal coordinate of the body, m
μ	=	dynamic viscosity, kg/m s
ρ	=	density, kg/m^3

Subscripts

aw	=	adiabatic wall condition
e	=	boundary-layer edge condition
w	=	wall condition
∞	=	freestream condition

Superscript

*	=	reference condition

Received 26 April 2000; revision received 1 November 2000; accepted for publication 5 November 2000.

*Assistant Professor, Department of Aerospace Engineering, 1 Hwayang-Dong Gwangjin-Gu. Member AIAA.
†Graduate Research Assistant, Department of Aerospace Engineering, 1 Hwayang-Dong Gwangjin-Gu.
‡Professor, Department of Aerospace Engineering, 1 Hwayang-Dong Gwangjin-Gu. Member AIAA.
§Assistant Professor, School of Aerospace and Mechanical Engineering, 98 Kunja-Dong, Gwangjin-Gu. Member AIAA.

Introduction

RECENTLY, there have been growing demands on small space launch vehicles for low-Earth-orbit satellites and next-generation launch vehicles such as reusable launch vehicles. From an aerodynamic perspective, efforts have been devoted to the study of a minimum-drag body, a body with minimum surface heat transfer rate, and an aerodynamic design of a high-speed propulsion nozzle. In early research, most of the studies implemented analytical or experimental approaches. In the 1980s and 1990s, the numerical approach was the major aerodynamic design tool with the advancement of computational fluid dynamics.

Minimum-drag bodies have been studied extensively since the 1950s. Zandbergen[1] and Parker[2] derived supersonic minimum-drag bodies using the method of characteristics and the linearized supersonic theory. In the hypersonic regime, Eggers et al.[3] derived a minimum-drag body with a small nose radius using Newtonian impact theory and showed that a power-law body ($R \sim x^n$) approximated the minimum-drag body when the power-law exponent n was 0.75. Mason and Lee[4] performed a numerical study to find an exponent of the minimum-drag power-law body using Euler equations. Zoby and Thompson[5] studied the effects of the nose radius and the angle of attack on a surface heat transfer and drag characteristics in hypersonic flow using a viscous shock-layer computer code.

Even though the drag and the surface heat transfer both are important in the design of space launch vehicles, studies on the minimum-drag body and the minimum surface heat transfer rate have been performed independently. There have been studies on the stagnation point heating, drag, and nose bluntness about power law shapes,[6] but less effort has been devoted to the design studies, which consider both drag and heat transfer characteristics together. In the present study, the representative shapes have been chosen from the nose fairing shapes of existing space launch vehicles, and the drag and the heat transfer characteristics have been investigated in the hypersonic flow regime of freestream Mach number $M_\infty = 5 \sim 8$. The minimum-drag body with a given surface heat flux constraint is designed with two well-known aerodynamic design methods, the inverse design and the numerical shape optimization. The inverse design is performed in conjunction with a parabolized Navier–Stokes (PNS) solver. In the numerical optimization, the modified Newtonian theory is applied, and internal volume is considered as a design constraint, in addition to surface heat flux, because payloads are accommodated in nose fairings. Three different gradient approximation techniques are tested and compared with each other. In addition, inverse design results are compared with those of numerical

optimization. An optimum nose fairing shape for the KSR-III (Korean Science Rocket III) space launch vehicle will be proposed.

Selection of Nose Faring Shapes and Drag/Heat Transfer Characteristics

Representative Nose Fairing Shapes of Space Launch Vehicles

Through analytical studies, many supersonic minimum-drag bodies have been derived. Among these, there are the von Kármán ogive (a given length and base radius) (see Ref. 7), the Sears–Haack body (a given length and volume) (see Ref. 7) and the Adams body (a given length, volume and, base radius) (see Ref. 8). In the hypersonic regime, there are the power-law body and the Hayes body (a given length and base radius). Mason and Lee[4] made numerical investigations using the Euler and PNS equations for both perfect gas and equilibrium air models. They concluded that the power-law body of $n = 0.69$ is a minimum-drag body for a given length and base radius in the supersonic and moderate hypersonic flow regimes ($M_\infty = 3 \sim 8$).

To analyze aerodynamic heating, which must be considered in hypersonic vehicle design, it is necessary to investigate the heat transfer characteristics of blunt bodies with finite nose radii. The amount of heat transfer is inversely proportional to a square root of nose radius, and so the nose bluntness has a considerable effect on the surface heat transfer, even though it has slight effect on the surface pressure distribution.

By investigating the existing space launch vehicles, four representative shapes, a cone–cylinder (shape I), a sphere–cone–cylinder (shape II), a sphere–power-law body (shape III), and an $n = 0.69$ power-law body (shape IV) were chosen. The numerical analyses for these shapes have been performed to understand the drag and the surface heat transfer characteristics.

Numerical Analysis Method

The compressible thin-layer Navier–Stokes equations are selected as the governing equations and Roe's flux difference splitting scheme is implemented for the spatial discretization with the MUSCL code for higher-order extension. The minmod limiter is used to remove solution oscillations. The global iteration was performed at the subsonic region near the nose tip, and the space-marching technique is employed for the fully supersonic region beyond the nose region to save computational cost. Laminar flow is assumed, and the convergence criterion of 10^{-5} is used. The computation was performed on the Cray C-90 supercomputer. The mesh is constituted with 91 stations along the axial direction i, 50 stations along the direction normal to the body axis k, and 2 stations along the circumferential direction j, which was verified to give reliable numerical solutions from the computational grid convergence test performed in the previous study.[4] For the numerical study, the three-dimensional computer code was run using only one slice of the full three-dimensional grid in the circumferential direction, with the boundary condition that there are no circumferential flow gradients. Freestream conditions were the conditions at altitude 40 km ($T_\infty = 260.9$ K and $p_\infty = 299.77$ N/m^2) and the constant wall temperature of 1000 K is used as the wall temperature boundary condition.

Pressure and Heat Transfer Distribution of Each Shape

Analysis calculations using PNS equations were performed at freestream Mach number 6.28 to find the pressure and the heat transfer characteristics of each shape. The results are shown in Fig. 1. Here, C_p is surface pressure coefficient, and the Stanton number C_h is given as $q_w/\rho_\infty u_\infty\ (H_{\text{aw}} - H_w)$. The pressures of shapes II, III, and IV (blunt bodies) increase rapidly near a nose tip. Both shape I (pointed nose tip) and shape IV (very small nose radius) have very large (a peak) heat transfer coefficient near the stagnation point. This means that shapes I and IV are not desirable when considering the surface heat transfer.

A total drag coefficient is the sum of a wave-drag and a skin-friction drag coefficients. The effect of Mach number to the total drag is shown in Fig. 2. As Mach number increases, the total drag coefficient decreases due to the decrease of wave-drag coefficient. Shapes I and II, with cylindrical afterbodies, have larger drags than

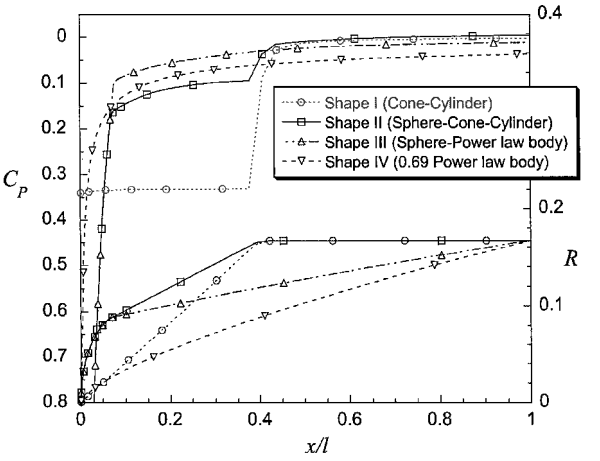

Surface pressure distributions

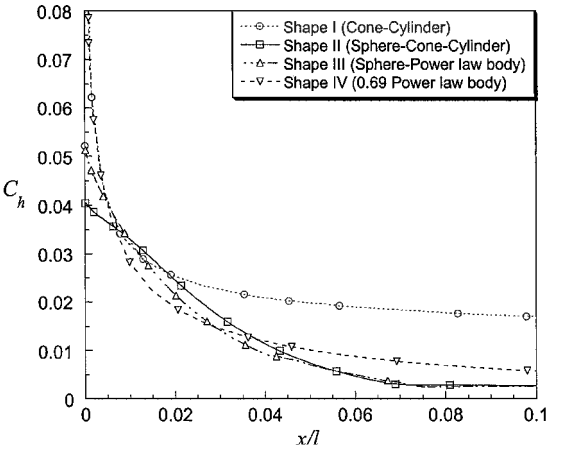

Local heat transfer rate distributions

Fig. 1 Pressure and local heat transfer rate distributions of several nose fairing shapes at freestream Mach number 6.28.

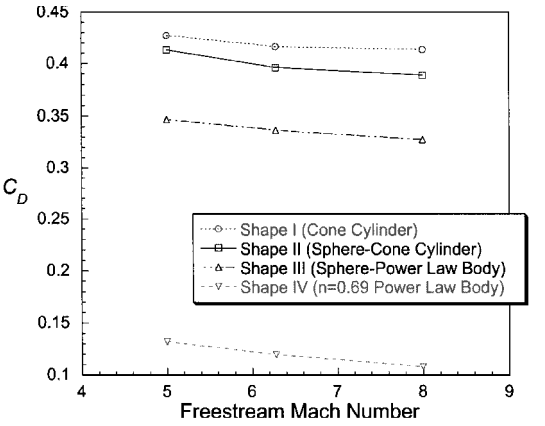

Fig. 2 Mach number effect on total drag of several nose fairing shapes.

the others. As far as the drag coefficient is concerned, shape IV is optimal, and shape II may be the best when considering the surface heat transfer because it shows lowest Stanton number near the stagnation point. When both drag coefficient and surface heat flux rate at the stagnation point are considered, shapes similar to shape III are best.

Inverse Design of Minimum-Drag Body with Given Heat Transfer Constraints

The aerodynamic design methods can be generally divided into two approaches: the numerical optimization and the inverse method. In the present study, the shock-expansion theory is applied to modify a body shape, and the convergence acceleration was attained with the regula-falsi method. Detailed descriptions of the inverse method for

the PNS equations and body geometry modifications are included in Ref. 9.

Space launch vehicles must have good drag and heat transfer characteristics. Shape III, which has a small drag coefficient and moderate heat transfer rate at the nose, is a promising nose fairing shape for the space launch vehicle operating in the Mach number range $M_\infty = 5 \sim 8$. Thus, the body, which has drag characteristics close to an $n = 0.69$ power-law body, a minimum-drag body at hypersonic speed, can be designed by selecting shape III as a nominal body geometry and the surface heat transfer rate as a design constraint. To meet the heat transfer constraint, a small portion near the nose tip must be fixed, and the design modification will be carried out in the remaining portion of the body. It is expected that the minimum-drag pressure distribution will exist in between the pressure distribution of the $n = 0.69$ power-law body and that of the nominal body (shape III). Thus, the two pressure distributions are averaged with a weighting factor, which is selected to satisfy the fineness ratio constraint $l/d = 3$.

Design Problem

The heat transfer coefficients of shapes II and III, which have blunt nose tips, do not exceed -0.06. Thus, the design problem 1 is formulated by selecting this value as a design constraint. The initial body is shape III, which has a finite nose radius of 0.091 (nondimensionalized by body length l) and a freestream Mach number of 6.28 with no angle of attack. The inverse design starts from $x/l = 0.04$. The target pressure distribution is identical with the $n = 0.69$ power-law body at $x/l = 0.04 \sim 0.07$ and is specified to satisfy the fineness ratio constraint at $x/l = 0.07 \sim 1.0$. The local Mach number is fixed[9] to the freestream Mach number M_∞, and the regula-falsi method is

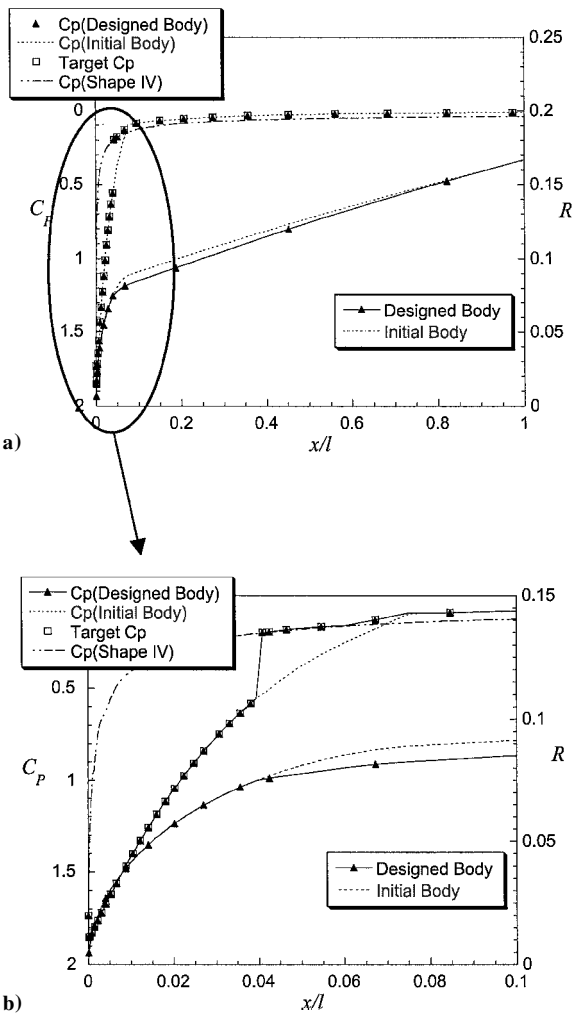

Fig. 3 Target pressure distribution and designed body at freestream Mach number 6.28: a) whole bodies and b) front 10% of the bodies.

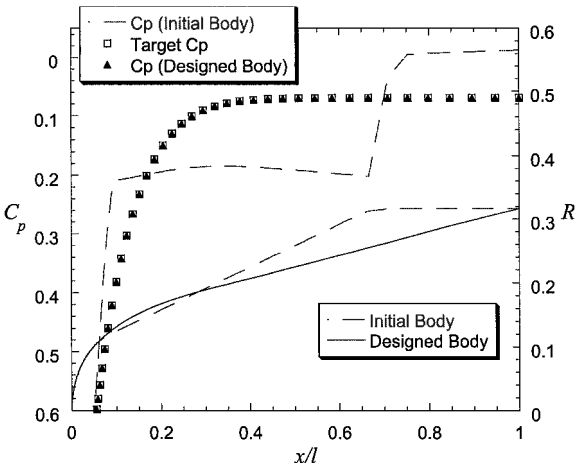

Fig. 4 Target pressure distribution and design body at freestream Mach number 4.6.

applied. The resultant body shape and the pressure distribution are shown in Fig. 3.

The designed body has about 6.5% less drag (wave drag 7% and skin-friction drag 4% reduced) than the initial body. The inverse-designed region shows a 22% reduction of drag and has 35% less drag than the minimum-drag body ($n = 0.69$ power-law body). The average number of design iterations per computational station is about 2.8.

KSR-III Design Improvement

The nose fairing shape of KSR-III is basically a sphere–cone–cylinder shape with a fineness ratio of 1.578 and a dimensionless nose radius of 0.087 (nondimensionalized by body length). The minimum-drag shape can be designed in the same way implemented in the preceeding design problem. The first-stage burnout (freestream Mach number 4.6 and altitude 31 km) is selected as the design condition. Wall temperature is fixed as 453 K, which is the operating temperature of the nose fairing. The inverse design starts from $x/l = 0.05$, and the target pressure distribution decreases quadratically from the starting point of the inverse design and has a minimum value at the end of the body. The value of the minimum pressure is adjusted to satisfy the fineness ratio. Figure 4 shows the designed body and the corresponding pressure distribution. The designed body has about 20.6% less drag (wave drag 20.9% and skin-friction drag 11.4%) than KSR-III. The heat transfer rate at the nose maintains the initial value.

Nose Fairing Shape Design Using Numerical Optimization

Design Statement

Generally, the inverse methods can find the body geometry within small design iterations or computational costs, but require the specification of the target pressure distributions and have difficulty handling the constraints imposed on the designed body.

To implement the inverse method for the aerodynamic performance improvement of the nose faring shape, some portion of the body must be fixed because the method is based on the space-marching problems. Hence, drag minimization may not be completed because we can not say that the shape obtained with considerable design improvements is the minimum. Moreover, the specification of the target pressure distribution is largely dependent on the design experience of the users, and application to the multipoint design or design with constraints is limited. To overcome these limitations, a numerical optimization technique is employed to find a body with minimum drag that satisfies a given surface heat flux at the nose.

Design Formulation

The nonlinear constrained optimization problem in this paper can be expressed as follows: Drag coefficient is the objective function in most cases. The surface heat transfer rate (the Stanton number C_h)

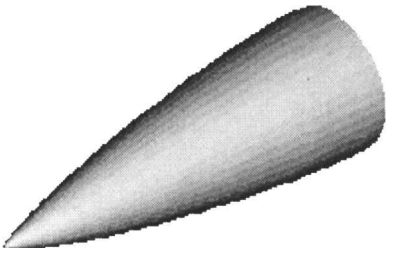

Kármán ogive

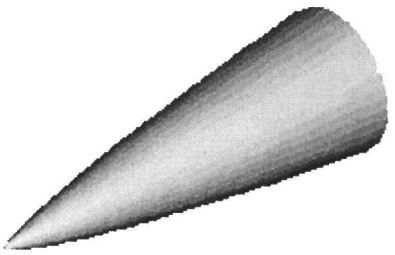

***n* = 0.69 power-law body**

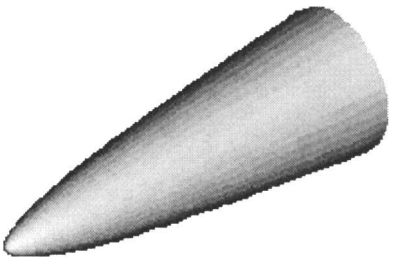

Paraboloid

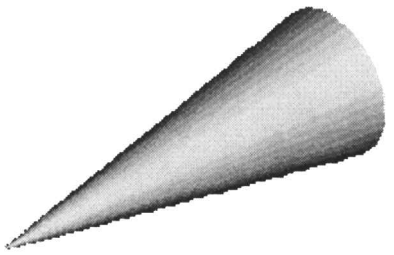

Sphere/cone

Fig. 5 Shape functions.

and the internal volume of the nose fairing are the inequality constraints, and the body fineness ratio is selected as an equality design constraint. As a side constraint, the move limit of the design variables is specified. These constraints are combined together or tested separately during the design optimization process.

According to Ref. 10, geometrically simple shapes are selected as shape functions, and the coefficients of the shape functions are the design variables. If some information about the body to be designed were available, this would be a very efficient approach because the number of design variables could be greatly reduced.

For the drag minimization of the space launch vehicle with specified heat flux and internal volume constraints, simple body shapes are selected as shape functions: Minimum-drag shapes include the von Kármán ogive, the power-law body with $n = 0.69$, and blunt shapes that have small surface heat transfer rates such as the paraboloid and sphere–cone. Each shape function is shown in Fig. 5.

In the optimization process, numerous evaluations of the objective functions and the design constraint functions and, hence, enormous computation time and cost are required. To reduce the computational efforts, the original objective function and constraints are approximated using the Taylor series expansion (see Ref. 11). The derived shape is analyzed to obtain the drag and surface heat flux. This completes one design cycle. When applying the approximate functions, the move limits of the design variables need to be considered as side constraints. Constraints about the body shape, for example, internal volume or fineness ratio, need not be approximated because those can be calculated analytically. For the present numerical optimization study, a simplex method is used for the linear problems (linear approximations to the objective function and design constraints). A reduced gradient algorithm with the quasi-Newton method is used for the nonlinear problems, in which the objective function and design constraints are approximated by the gradients and the Hessain matrix. The shape optimization procedure is shown in Fig. 6.

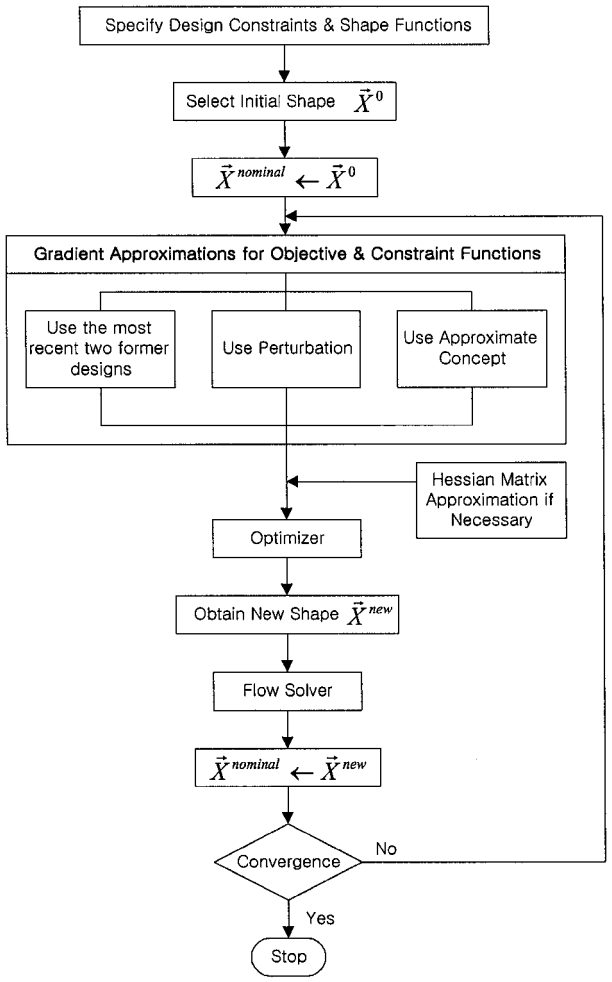

Fig. 6 Shape optimization procedure.

Gradient Approximation and Design Strategy

Gradient terms are included in the linear approximations of the objective function and the design constraints. Because the gradient not only shows the direction of the solution but also determines the accuracy of the linearized functions, it has a great effect on the design convergence and the solutions. When the gradients are not correct, either the design space does not exist or the shapes with severe constraint violations are derived. The gradients are easily obtained using a finite difference approximation. In this study, three different methods are considered.

For method 1, the gradient is obtained using the difference between the nominal shape and the shape derived from the previous design cycle. To obtain the gradient information about each design variable, the same number of analysis calculations as the number of design variables is required in each design cycle. For method 2 (perturbation), corresponding changes of the functions are calculated with the small perturbation to the nominal shape. This case also requires the same number of analysis calculations as method 1. The strong point of this approach is that the approximations of the local gradients about the nominal shape, as well as the linearized function, are relatively accurate. Finally, for method 3 (the approximation concept), gradients can be determined by expressing the difference between the shape functions and nominal shapes as a linear system of equations.[11] Initial analysis calculations for each

shape function and exactly one additional analysis run per design iteration are required to proceed with the design. Hence, the computational efforts can be greatly reduced. In addition, this method has the advantage that higher-order terms such as Hessian terms, as well as the gradient terms, can be included easily as the design proceeds. The weak point is that the gradient information can be inaccurate when the designed body and nominal body shapes are very different; hence, the number of design cycles may be increased.

The design convergence and the accuracy of the approximated function are largely dependent on the move limit of the design variables. For unconstrained problems, a relatively large move limit can be assigned to accelerate the convergence, and for constrained problems, a small move limit is used because the accuracy of the constraint functions is important.

When utilizing mutually conflicting functions as the objective and constraint functions (such as drag and surface heat flux), or when the feasible design space is very narrow because the constraints are very severe, the optimization may not be straightforward. In those cases, a two-step optimization can be employed, that is, minimize the constraints to the allowable values first, then minimize the original objective function while maintaining the constraint values.

Analysis Methods

Because the numerical optimization process requires a large number of iterative analysis calculations, it is very costly to employ accurate analysis methods that require a large amount of computational time. For the design strategy definition and in the preliminary design optimization stage it is better to employ relatively simple analysis methods approximating the accurate analysis, if available. For the wave drag approximation in the hypersonic flow regime, tangent-cone theory (TCT), shock-expansion theory, or modified Newtonian theory (MNT) can be used. In the present study, a surface pressure distribution is determined by either modified Newtonian theory or tangent-cone theory. There are no restrictions on the particular choice of the methods for the given design optimization problems. A surface temperature is determined by using the entropy relation across the normal shock and an isentropic flow assumption between the shock and stagnation point.[12] After the surface pressure and temperature are determined, other thermodynamic and flow properties can be determined.

By using the Zoby et al. approximate convective heating equation,[13] the heat flux at the stagnation point is calculated. The laminar heat transfer rate is given by

$$\dot{q}_{w,L} = 0.22 R_{\theta,e}^{-1}(\rho^*/\rho)(\mu^*/\mu)\rho_e u_e (H_{\text{aw}} - H_w) Pr_w^{-0.6} \qquad (1)$$

where R_θ is momentum thickness Reynolds number. Here, the momentum thickness is evaluated at the grid point next to the stagnation point, where θ goes to zero. The asterisk denotes conditions determined by reference enthalpy. The Stanton number at the stagnation point is shown as a function of the nose radius in Fig. 7. When compared with the results from thin-layer Navier–Stokes analyses, the approximate equation produces qualitatively agreeable solutions.

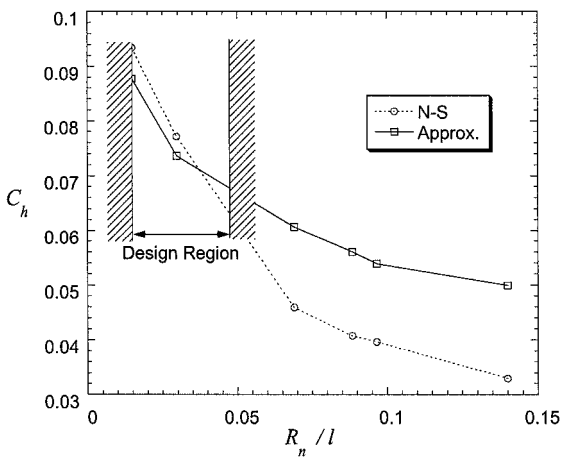

Fig. 7 Comparison of the approximated surface heat flux prediction with detailed analysis at freestream Mach number 6.28.

Table 1 Comparison of cases 1–4

Case	Initial shape	Gradient approximation	Wave drag (TCT/MNT)
1	Paraboloid	Method 1	0.0518/0.0450
2	Paraboloid	Perturbation	0.0556/0.0437
3	Combination	Perturbation	0.0542/0.0446
4	Combination	Approximation concept	0.0587/0.0464

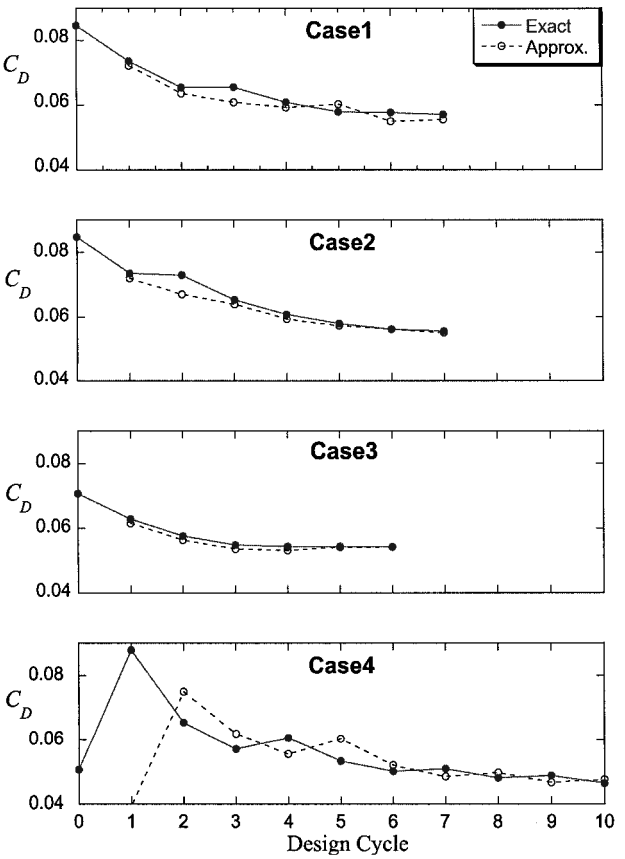

Fig. 8 Convergence behaviors of cases 1–4 at freestream Mach number 6.28.

Wave Drag Minimization

To check the validity of the shape functions selection and the gradient approximations, the wave drag minimization with a fineness ratio (l/d) constraint has been performed. The selected shape functions are the von Kármán ogive, $n = 0.69$ power-law body, cone, and paraboloid. The constraint is the fineness ratio of three. The surface pressure has been determined by tangent-cone theory. The results, assuming several different initial shapes and gradient approximations, are compared and summarized in Table 1 and Fig. 8. In cases 1 and 2, the paraboloid of fineness ratio three is used for the initial shape, and the gradient vector is determined by methods 1 and 2, respectively. To check the convergence behavior when starting from different initial shapes, case 3 used the combination of shape functions as an initial geometry. In case 4, the sphere-cone instead of the cone is used as a shape function, and the combination of four shape functions is used for the initial shape. The gradient approximation method 3 and the modified Newtonian theory have been used in case 4. As shown in Fig. 8, the values of wave drag are converged to nearly the same value, 0.0536, which is the wave drag of the $n = 0.69$ power-law body, the minimum drag shape in supersonic speed, even though the different gradient approximation methods are applied. The exact value in Fig. 8 is the result of the simple analysis method employed in this study. As the design converges, the approximated value using the first- or second-order Taylor series expansion and the exact value approach one another. The gradient approximation method 2 is the most accurate, and the

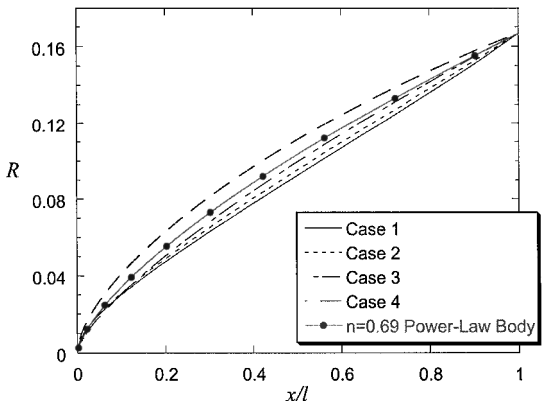

Fig. 9 Designed bodies of cases 1–4 at freestream Mach number 6.28.

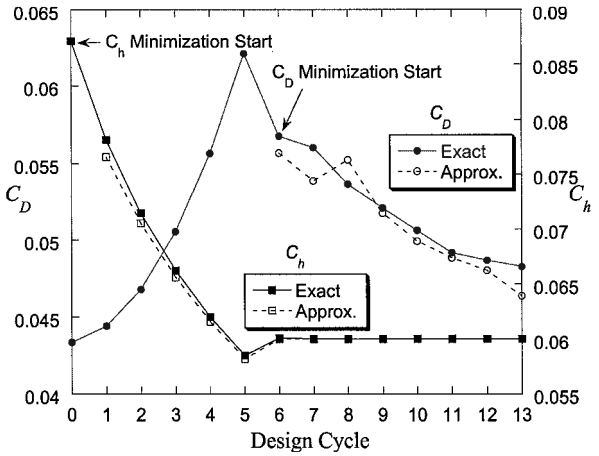

Fig. 10 Convergence behavior of two-step approach at freestream Mach number 6.28.

approximation method 3 requires only one-quarter of the analysis runs required by other cases. In case 4, drag reduction after 10 design cycles is less than other cases because the sphere–cone, selected as a shape function has an adverse effect on the wave drag minimization. This example case demonstrates the importance of the shape function selection. Figure 9 shows the designed shapes of cases 1–4. All cases have almost the same value as the wave drag, but have different shapes. The inherent existence of local optima in the wave drag can be resolved by specifying the heat transfer rate constraints, which will be shown in the next section.

Wave Drag Minimization with Surface Heat Transfer Constraints

In this case, the wave drag minimization is performed with a given surface heat transfer constraint in addition to the geometric constraint, fineness ratio. Because a sharp nose cone is not adequate in the region of high heat transfer rate, the sphere–cone is used as a shape function. The surface pressure is determined by modified Newtonian theory. A Stanton number of 0.06 is specified as a constraint, and this value is less than that of any shape function. To facilitate the optimization, a two-step approach is implemented. First, the constraint, the Stanton number, is minimized to the value below 0.06. Then the wave drag minimization follows with the resulting shape of the heat transfer minimization as an initial shape. The designed body and the convergence behavior are shown in Figs. 10 and 11. The shape obtained from the numerical optimization is much different than the result of the inverse design problem that has a fixed portion near the nose because no restrictions to the body geometry are imposed. The drag of the optimized shape is 80% less than that of the inverse-designed shape. The result suggests that, at the expense of the computational time and cost, the numerical shape optimization, especially in the constrained design problems with well-selected shape functions, has a better capability of finding an optimum shape than the inverse design in which the shape is determined only by target pressure.

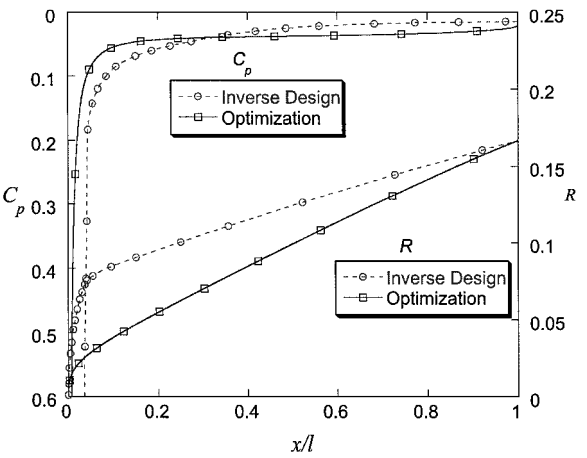

Fig. 11 Designed bodies using the inverse method and numerical optimization at freestream Mach number 6.28.

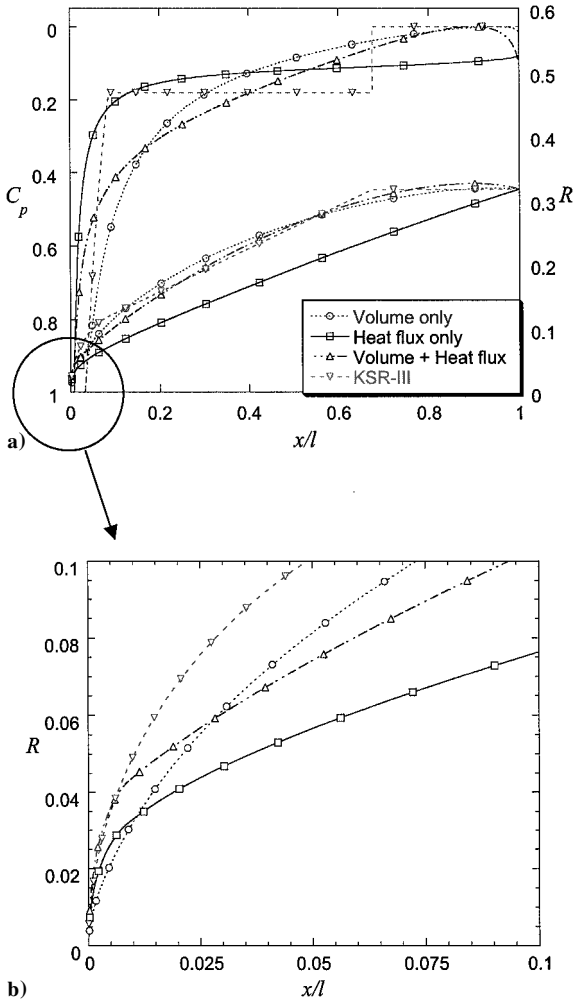

Fig. 12 Comparison of the designed bodies and pressure distributions according to different design constraints (M_∞ = 4.6): a) whole bodies and b) front 10% of bodies.

However, much better results or designs can be expected with proper treatment of the inverse methods such as target pressure optimization.

The second design problem is the wave drag minimization of KSR-III. As an inequality constraint, the surface heat transfer of KSR-III baseline, $C_h = 0.0137$, is selected, and an equality constraint is the fineness ratio of KSR-III baseline, $l/d = 1.578$. The design conditions are a freestream Mach number of 4.6 and an altitude of 31 km. A shape, which has 53% less drag than KSR-III, is obtained after seven design cycles. It is shown in Fig. 12. To satisfy

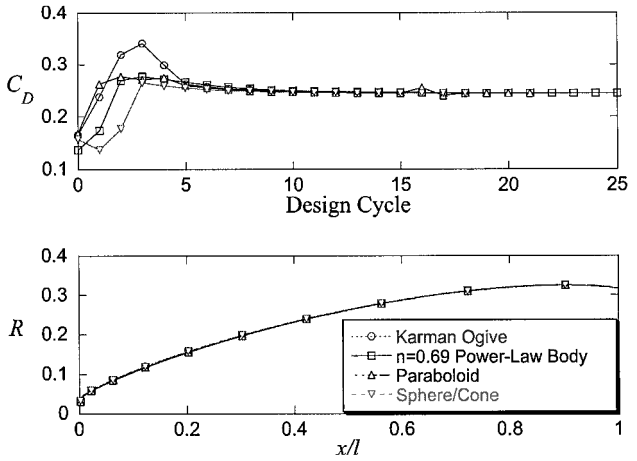

Fig. 13 Design results starting from various initial shapes at freestream Mach number 4.6.

the surface heat transfer constraint, the shape has nearly the same nose radius as KSR-III.

Wave Drag Minimization with Surface Heat Transfer and Internal Volume Constraints

In the actual design of the nose fairing, internal volume is also a very important design parameter, in addition to the drag and surface heat transfer rate, because the design requirement dictates a sufficient internal volume to accommodate payloads like satellites or observational instruments. Thus, the internal volume of 0.1989, nondimensionalized by l^3, is selected as a design constraint in addition to the surface heat transfer and fineness ratio. The shape functions are the same as the preceding cases with different fineness ratios. The design conditions are also the same. The volume of KSR-III is much larger than that of any shape functions; hence, the initial shape is selected to satisfy the volume constraint.

After 15 design cycles with the gradient approximation method 2, the designed body has about 18% less wave drag than KSR-III. With or without surface heat transfer and internal volume constraints, the design results are shown in Fig. 12. The front 10% of the designed shapes are enlarged in Fig. 12. With the surface heat transfer constraint, the nose radii remain finite values. When only the internal volume is considered as a design constraint, the designed body has smaller nose radius than the case with the surface heat transfer constraint.

To overcome the drawback of the gradient-based optimization methods of reaching the local minimum, the designs starting from various initial shapes are examined, and the results are shown in Fig. 13. Each case has a different convergence rate, but the designed bodies and their wave drag correspond with each other.

Conclusions

Two design approaches, the inverse method and the numerical optimization, have been successfully implemented in the design of the space launcher. Though the numerical optimization shows better design results in this study, improved design results can also be expected with proper treatment of inverse methods such as target pressure optimization. In addition, the inverse design requires very small computational costs.

From the inverse design with the heat transfer constraint, the following conclusions can be drawn: By the specification of the nose radius, it was demonstrated that the inverse method can be used for a shape design with less drag with a given surface heat transfer constraint. With only two or three design iterations at each computational plane, the body that has much less drag than the initial shape, which satisfies design constraints of the maximum Stanton number at the stagnation point and the fineness ratio $l/d = 3$, is successfully designed. While maintaining the initial stagnation heat flux, a body with considerably less drag than KSR-III was designed using the method. The inverse method produces the body, which has about 21% less wave drag than the KSR-III's baseline at a freestream Mach number of 4.6. Even though the inverse method can not derive the real minimum drag shape, it can be used for design improvements with relatively small computational cost.

From the numerical shape optimization study with various design constraints, the following conclusions can be drawn: From the optimization with the design constraints for the fineness ratio and the surface heat transfer rate, the effects of gradient approximations, the move limit of design variables, shape functions, and initial shapes are investigated, and the convergence behaviors are evaluated. Compared with the inverse method, the numerical optimization shows efficiency for the constrained design problems and produces better results: a shape with 53% less drag than the baseline geometry of KSR-III was obtained.

By the selection of the fineness ratio and internal volume of the nose fairing as design constraints, the shape, which has 13% less wave drag and 28% less heat transfer at the stagnation point than KSR-III, is obtained through the two-step approach. With the fineness ratio, surface heat transfer, and internal volume as simultaneous constraints, the shape, which has 18% less wave drag than the KSR-III baseline, is designed. Through the several design examples described, it was demonstrated that the developed method could be used in practical design problems with various design constraints.

Acknowledgment

This study was supported by Konkuk University in 1999.

References

[1]Zandbergen, P. J., "On the Determination of Optimum Shapes with Finite Nose Angles," National Aero and Astronautical Research Inst., Rept. NLR-TR G.30, Amsterdam, July 1964.

[2]Parker, H. M., "Minimum-Drag Ducted and Pointed Bodies of Revolution Based on Linearized Supersonic Theory," NACA Rept. 1213, 1955.

[3]Eggers, A. J., Jr., Resnikoff, M. M., and Dennis, D. D., "Bodies of Revolution Having Minimum-Drag at High Supersonic Airspeeds," NACA Rept. 1306, Jan. 1957.

[4]Mason, W. H., and Lee, J.-W., "Minimum Drag Axisymmetric Bodies in the Supersonic/Hypersonic Flow Regimes," *Journal of Spacecraft and Rockets*, Vol. 31, No. 3, 1994, pp. 406–413.

[5]Zoby, E. V., and Thompson, R. A., "Flowfield and Vehicle Parameter Influence on Hypersonic Heat Transfer and Drag," *Journal of Spacecraft and Rockets*, Vol. 27, No. 4, 1990, pp. 361–368.

[6]O'Brien, T. F., and Lewis, M. J., "Power-Law Shapes for Leading-Edge Blunting with Minimal Shock Standoff," *Journal of Spacecraft and Rockets*, Vol. 36, No. 5, 1999, pp. 653–658.

[7]Ashley, H., and Landahl, M., *Aerodynamics of Wings and Bodies*, Dover, New York, 1965, pp. 178–181.

[8]Ramaswamy, M. A., and Viswanathan, S., "Some Observations on the Adams Body of Minimum Wave Drag," *Journal of Aircraft*, Vol. 12, No. 12, 1975, pp. 1001, 1002.

[9]Lee, Y.-K., and Lee, J.-W., "Viscous Inverse Method for the High-Speed Axisymmetric Body Design," AIAA Paper 98-4806, Sept. 1998.

[10]Vanderplaats, G. N., and Hicks, R. M., "Numerical Airfoil Optimization Using a Reduced Number of Design Coordinates," NASA TM X-73151, July 1976.

[11]Vanderplaats, G. N., "Approximation Concepts for Numerical Airfoil Optimization," NASA TP 1370, March 1979.

[12]Moore, F. G., Armistead, M. J., Rowles, S. H., and DeJarnette, F. R., "New Approximate Method for Calculating Real Gas Effects on Missile Configurations," *Journal of Spacecraft and Rockets*, Vol. 30, No. 1, 1993, pp. 22–31.

[13]Zoby, E. V., Moss, J. N., and Sutton, K., "Approximate Convective-Heating Equations for Hypersonic Flows," *Journal of Spacecraft and Rockets*, Vol. 18, No. 1, 1981, pp. 64–70.

T. C. Lin
Associate Editor